THE NUMERICAL ANALYSIS OF THE AEROELASTIC BEHAVIOUR FOR A TURBOMACHINE BLADE ROW IN 3D VISCOUS FLOW

Gnesin V.I. and Kolodyazhnaya L.V.
Department of Aerohydromechanics Institute of Mechanical Engineering Problems
National Academy of Sciences of Ukraine, 2/10 Pozharsky st., Kharkov, 61046 Ukraine
E-mail: gnesin@ipmach.kharkov.ua

Rzadkowski R.
Department of Dynamics of Machines Institute of Fluid Flow Machinery Polish Academy of Sciences
J. Fiszera st.,14, Gdansk, 80 952 Poland
E-mail: z3@imp.gda.pl

ABSTRACT

In this study a three-dimensional nonlinear time-marching method and numerical analysis for aeroelastic behaviour of oscillating blade row has been presented. The approach is based on the solution of the coupled fluid-structure problem in which the aerodynamic and structural equations are integrated simultaneously in time.

The unsteady Reynolds-averaged Navier-Stokes (RANS) solver coupled with modified Baldwin and Lomax algebraic eddy viscous turbulence model, is applied to calculate three-dimensional unsteady viscous flow through the vibrating rotor blade row. The structure analysis uses the modal approach and 3D finite element model of a blade. The code is proven to be accurate and efficient by computing the 11th Aeroelastic Standard Configuration, namely subsonic and transonic flow through a turbine cascade at design and off-design conditions. Comparison of the calculated and experimental results has shown sufficient quantitative and qualitative agreement for local performances (unsteady pressure amplitude and phase distribution). The numerical analysis of 3D unsteady viscous flow through the last turbine stage rotor blade row is presented.

1. INTRODUCTION

In modern turbomachinery design and development it is important to predict the aeroelastic behaviour of blades. This is true not only for aircraft compressor and fan blade rows, but also for the last stages of steam and gas turbines that work at highly loaded off-design conditions.

The prediction of the unsteady pressure loads and aeroelastic behaviour of blades may involve the computation of shock waves, shock/boundary layer interaction and boundary layer separation, which could not be accounted in frame of inviscid methods. In order to overcome this limitation complete Reynolds-averaged Navier-Stokes (RANS) equations are to be used to model complex and off-design cases of turbomachinery flows.

The unsteady prediction models for 3D viscous flutter have been discussed in literature over the last ten years (Sayma et al, 1998; Weber et al, 1998; Vasanthakumar et al, 2001; Chassaing and Gerolymus, 2001; Cinnella et al, 2004).

The aim of this study is to present the numerical method for discretizing of Navier-Stokes equations by using the second order by time and coordinates explicit finite-volume Godunov's type difference scheme, and moving hybrid H-O structured grid.

In the present study the 3D Reynolds-averaged Navier-Stokes (RANS) solver, coupled with modified Baldwin and Lomax's algebraic eddy viscous turbulence model, is applied to calculate three-dimensional unsteady viscous flow through the vibrating steam turbine blade row.

The structure analysis uses the modal approach and 3D finite element model of a blade.

To validate the numerical viscous code developed there was performed the comparison the numerical calculations results with the measure data for 11th International Standard Configuration, which represents a turbine blade geometry, and with the calculated results of other authors presented in works (Fransson et al, 1999; Cinnella et al, 2004). The comparison has shown sufficient quantitave and qualitative agreement for local unsteady performances (pressure amplitude and phase distribution).

The numerical analysis results of aeroelastic behaviour for the rotor blade row of the steam turbine last stage for nominal and off-design regime were presented.

2. GOVERNING EQUATIONS

The full system of unsteady compressible Reynolds-averaged Navier-Stokes (RANS)

equations expressing the conservation laws, can be presented in Cartesian coordinate system rotating with a constant angular velocity ω as follows:

$$\frac{\partial U}{\partial t}+\frac{\partial E}{\partial x}+\frac{\partial F}{\partial y}+\frac{\partial G}{\partial z}+H=\frac{\partial R}{\partial x}+\frac{\partial S}{\partial y}+\frac{\partial Q}{\partial z}, \quad (1)$$

where U - is the symbolic vector of conservative variables; E, F, G and R, S, Q are inviscid and viscous flux vectors respectively; H is the source term caused by uninertial coordinate system

$$U=\begin{pmatrix}\rho\\ \rho\upsilon_1\\ \rho\upsilon_2\\ \rho\upsilon_3\\ h\end{pmatrix};\quad E=\begin{pmatrix}\rho\upsilon_1\\ p+\rho\upsilon_1^2\\ \rho\upsilon_1\upsilon_2\\ \rho\upsilon_1\upsilon_3\\ (h+p)\upsilon_1\end{pmatrix};\quad F=\begin{pmatrix}\rho\upsilon_2\\ \rho\upsilon_2\upsilon_1\\ p+\rho\upsilon_2^2\\ \rho\upsilon_2\upsilon_3\\ (h+p)\upsilon_2\end{pmatrix};$$

$$G=\begin{pmatrix}\rho\upsilon_3\\ \rho\upsilon_3\upsilon_1\\ \rho\upsilon_3\upsilon_2\\ p+\rho\upsilon_3^2\\ (h+p)\upsilon_3\end{pmatrix};\quad R=\begin{pmatrix}0\\ \tau_{xx}\\ \tau_{xy}\\ \tau_{xz}\\ \beta_x\end{pmatrix};\quad S=\begin{pmatrix}0\\ \tau_{yx}\\ \tau_{yy}\\ \tau_{yz}\\ \beta_y\end{pmatrix};$$

$$Q=\begin{pmatrix}0\\ \tau_{zx}\\ \tau_{zy}\\ \tau_{zz}\\ \beta_z\end{pmatrix};\quad H=\begin{pmatrix}0\\ \rho a_e^1-2\rho\omega\upsilon_2\\ \rho a_e^2+2\rho\omega\upsilon_1\\ 0\\ 0\end{pmatrix};$$

a_e^1, a_e^2 are the transfer acceleration projections; $h=\rho\left(\frac{1}{k-1}\frac{p}{\rho}+\frac{\upsilon_1^2+\upsilon_2^2+\upsilon_3^2-r^2\omega^2}{2}\right)$ is rothalpy;

$$\beta_x=\upsilon_1\tau_{xx}+\upsilon_2\tau_{xy}+\upsilon_3\tau_{xz}+\lambda\frac{\partial T}{\partial x};$$

$$\beta_y=\upsilon_1\tau_{yx}+\upsilon_2\tau_{yy}+\upsilon_3\tau_{yz}+\lambda\frac{\partial T}{\partial y};$$

$$\beta_z=\upsilon_1\tau_{zx}+\upsilon_2\tau_{zy}+\upsilon_3\tau_{zz}+\lambda\frac{\partial T}{\partial z}.$$

Here p is pressure; ρ is density; υ_1, υ_2, υ_3 are the velocity components; τ_{ij} (i,j=x,y,z) are the viscous stress tensor components given by

$$\tau_{ij}=\begin{cases}\mu\left(\frac{\partial\upsilon_i}{\partial x_j}+\frac{\partial\upsilon_j}{\partial x_i}\right) & if\ \ i\neq j\\ 2\mu\frac{\partial\upsilon_i}{\partial x_i}-\frac{2}{3}\mu\, div\vec{\upsilon} & if\ \ i=j\end{cases};$$

μ is the dynamic viscosity coefficient; λ is heat conduction coefficient.

The system of equations (1) is completed with the perfect gas law equation $\varepsilon=\frac{1}{\gamma-1}\frac{p}{\rho}$, where γ is the adiabatic exponent (specific heat ratio).

In this study it was applied the algebraic turbulence model based on the original two-layer model (Cebeci and Smith, 1974) and modified by Baldwin and Lomax (Baldwin and Lomax, 1978).

A multipassage computational domain includes a number of blade passages $n\geq 1$ depending from interblade phase angle of oscillations (IBPA) that provides flow periodicity conditions:

$$n=\frac{360^\circ\cdot z}{|IBPA|},\quad IBPA\neq 0,$$

where z is the minimum integer which leads to an integer value for n. Each of passages includes a blade and has an expansion in the circumferential direction, which is equal to the pitch of a blade row. The three-dimensional grid consists of a sequence of two-dimensional grids that are stacked together in the radial direction from hub to tip. The two-dimensional grids are similar and discretized using hybrid H-O grid (Figure 1). The external H-grid remains fixed during the calculation while O-grid is rebuilt in each iteration according to the blade moving.

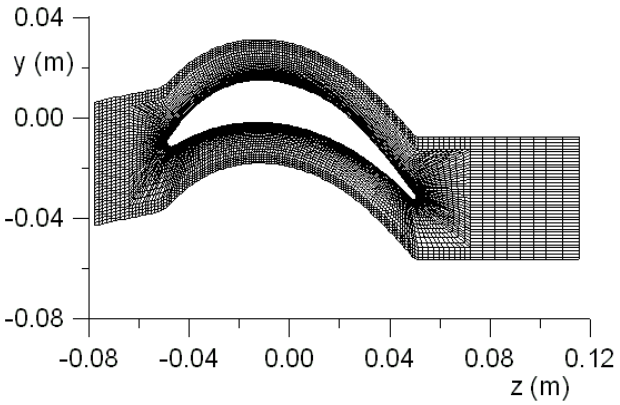

Figure 1: *Viscous mesh, inner O-mesh, outer H-grid.*

For the most of flows under the high Reynolds numbers the flow field at the infinity from solid body looks like ideal gas flow. So for turbomachinery calculations boundary conditions at the inlet and outlet of the computational domain are based on the theory of characteristics for unsteady one-dimensional problem as in case of Euler equations. Assuming that the axial flow velocity is subsonic at the inlet and outlet of the cascade, boundary conditions are established by replacing incoming waves with fixed flow values, i.e. the total pressure, total temperature and flow angles are

imposed at the inlet boundary while the static pressure is kept constant at the outlet boundary.

At a solid wall the so called no-slip condition is given by $\overline{\upsilon} = \overline{\upsilon}_w$, where $\overline{\upsilon}_w$ is wall velocity in the considered reference system.

For the temperature either the wall temperature is fixed $T = T_w$ or the heat flux is determined by the physical conditions, that is

$$q_w = -\lambda \frac{\partial T}{\partial n}.$$

For an adiabatic wall $q_w = 0$.

The second thermodynamic variable at the solid wall can be obtained from the momentum equation projected on the normal direction to the wall, which reduces to

$$\frac{\partial p}{\partial n} = grad_n \tau .$$

Equations (1) are written for each cell of the computational mesh following to Godunov's idea (Godunov at al, 1976) but in more universal form for an arbitrary moving three-dimensional difference grid (Gnesin at al, 2004):

$$\begin{aligned}&\frac{1}{2\Delta t}[3U^{n+1}\Omega^{n+1} - 4U_n\Omega_n + U_{n-1}\Omega_{n-1}] + \\ &+\left[\left(-U w_n + E - R\right)\sigma\right]_{i+1} - \left[\left(-U w_n + E - R\right)\sigma\right]_i + \\ &+\left[\left(-U w_n + F - S\right)\sigma\right]_{j+1} - \left[\left(-U w_n + F - S\right)\sigma\right]_j + \\ &+\left[\left(-U w_n + G - Q\right)\sigma\right]_{k+1} - \\ &-\left[\left(-U w_n + G - Q\right)\sigma\right]_k + H_n\Omega_n = 0\end{aligned} \qquad (2)$$

Here subscripts and superscripts correspond to "old" and "new" cells; σ and w_n are the area and normal velocity of "middle" side. The gasdynamic parameters on the lateral sides (expressions in square brackets with integer indices) are defined by the solving of the problem about the break-down (Riemann problem) of an arbitrary discontinuity on the moving interfaces between two adjacent cells by using a piecewise linear approximation of parameters in grid cells. Constructed in this way the difference scheme is a monotonic scheme, and it has second-order accuracy on the smooth solutions with respect to spatial and time coordinates.

The dynamic model of the oscillating blade with use of the modal approach reduces to a set of decoupled differential equations relatively to modal coefficients of natural modes:

$$\ddot{q}_i(t) + 2h_i\dot{q}_i(t) + \omega_i^2 q_i(t) = \lambda_i(t). \qquad (3)$$

Here h_i –mechanical damping i-mode coefficient; ω_i – natural i-mode frequency; λ_i – modal force relative to i-mode displacement, calculated at every iteration by instant pressure distribution on blade surface

$$\lambda_i = \frac{\iint_\sigma p\overline{U}_i \cdot \overline{n}^\circ \, d\sigma}{\iiint_v \rho \overline{U}_i^2 \, dv},$$

where p – blade surface pressure.

Having defined the modal coefficients q_i from the system of differential equations (3), blade displacement and velocity are obtained as

$$u(x,t) = \sum_i U_i(x) q_i(t), \quad \dot{u}(x,t) = \sum_i U_i(x) q_i(t).$$

3. NUMERICAL ANALYSIS

The numerical verification of the method presented has been performed for the 11th Standard Configuration (Fransson et al, 1999). Three selected experiments are proposed as test cases: one subsonic case ($M_2 = 0.69$) for code calibration, one transonic off-design case with high incidence inlet flow angle ~18 deg ($M_2 = 0.99$) and a separation bubble on the suction surface, and supersonic off-design case ($M_2 = 1.42$) with incidence flow angle ~33 deg. The details of these cases including full blade geometry are given in work (Fransson et al, 1999).

Viscous computations have been performed using O-grids with 390×42 cells, and the average value of y^+ for the first cell near the wall was about 1.0.

Figure 2 shows the comparison of predicted steady results for subsonic case in terms of isoentropic Mach number distribution. It demonstrates a smooth change of flow over the blade surfaces without remarkable disturbances. The integer "1" corresponds to the method presented results, the integer "2" corresponds to the experimental results, and the integer "3" corresponds to calculated results, received with use of VOLFAP code (unsteady quasi-3D viscous flow code for Navier-Stokes equations) and presented in work (Fransson et al, 1999).

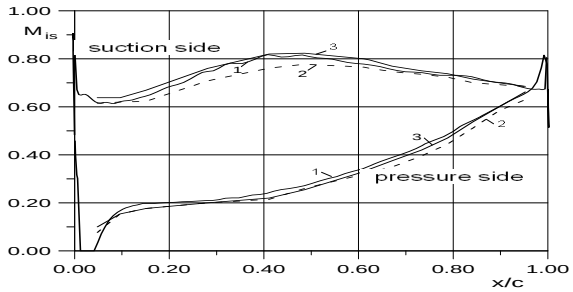

Figure 2: *Mach number distribution, midspan, off-design transonic case, M_{2is} = 0.69*

The calculations show the sufficient agreement with experimental data and VOLFAP code. Some deviation occurs in the middle of the blade on suction side compared to the experiment.

Reasons for the deviations between experimental data and numerical results may be found in real flow effects which cannot be captured by the applied numerical model or are lost due to the measuring technique (for example inaccuracies in measurement of pressure, estimation of flow angles, averaging of flow values over pitch and span).

Also the off-design calculations show in Figure 3 sufficient agreement with experimental data with exception of the shock prediction. The shown off-design case indicates a separation bubble to be present from leading edge to 30% of true chord (see Figure 4) and a shock at about 80% of true chord, whereas the experiment shows it to be at around the 65% mark. It should be noted that only the viscous code can predict the separation bubble indicated by the deceleration which occurs on 15-25% relative chord on suction side.

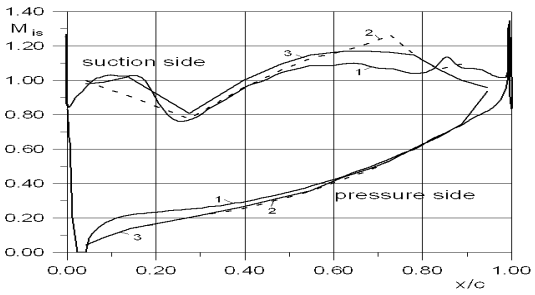

Figure 3: *Mach number distribution, midspan, off-design transonic case, M_{2is} = 0.99*

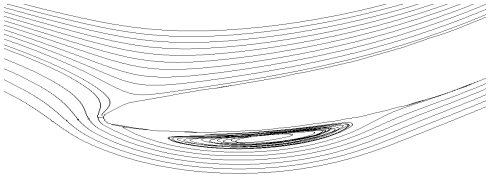

Figure 4: *The streamlines near the leading edge, M_{2is} = 0.99*

Finally Figure 5 shows the sufficient agreement between calculated results and experimental data for regime M_{2is} = 1.42 and incidence angle β = 33 deg.

The numerical model demonstrates the sufficient prediction of Mach number distribution over the blade surface and shock position on the suction side.

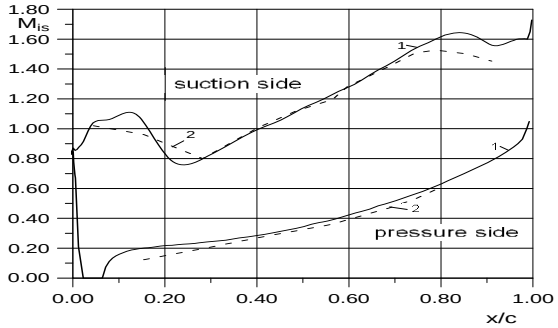

Figure 5: *Mach number distribution, midspan, off-design transonic case, M_{2is} = 1.42*

For the unsteady case (transonic regime $M_2 = 0.99$) the blades oscillate in the first bending mode with bending angle equal to 90 deg with respect to the chord direction, oscillation amplitude equal to 0.0035 of chord length, and a reduced frequency equal to 0.1545.

The presented results are obtained from a Fourier transformation of the unsteady time domain solution

$$C(t) = C_0 + \sum_{n=1}^{\infty} (C_{1n} \cos n2\pi\nu t + C_{2n} \sin n2\pi\nu t)$$

where $C(t)$ is a physical quantity under study; C_0, C_{1n}, C_{2n} are the Fourier series coefficients; ν is a vibration frequency.

The pressure coefficients in amplitude and phase are defined by formulas

$$C_p(x) = \frac{p(x)c}{(p_0 - p_1)h},$$

$$p(x) = \sqrt{C_{1n}^2(x) + C_{2n}^2(x)}, \quad \varphi(x) = arctg\frac{C_{2n}(x)}{C_{1n}(x)}$$

where $p(x)$ is amplitude of nonstationary pressure along the blade; $\varphi(x)$ is a phase; p_0 and p_1 are the total and static pressure at the inlet of cascade; c is a chord length; h is amplitude of bending oscillations.

Only the first harmonics of the pressure response are compared in terms of amplitude and phase. In the nonlinear results higher harmonics had nearly no influence.

The nonstationary aeroelastic characteristics of the 11th Standard Configuration for the transonic off-design case are demonstrated in Figures 6,7.

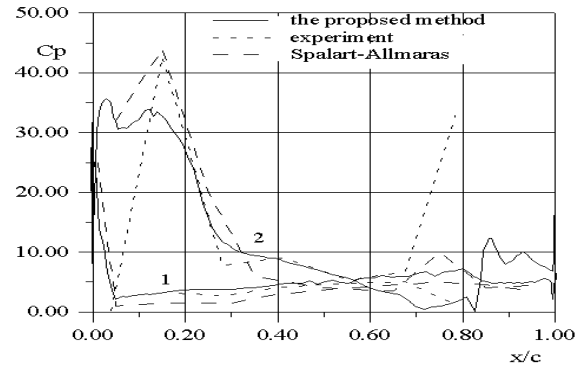

(a) amplitude

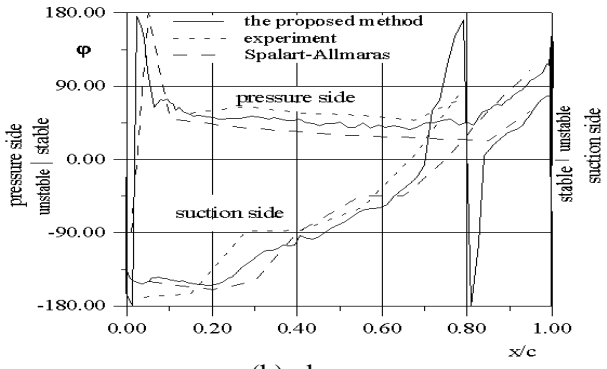

(b) phase

Figure 6: *The amplitude and phase of the 1st harmonic for unsteady pressure coefficient, IBPA=144 deg*

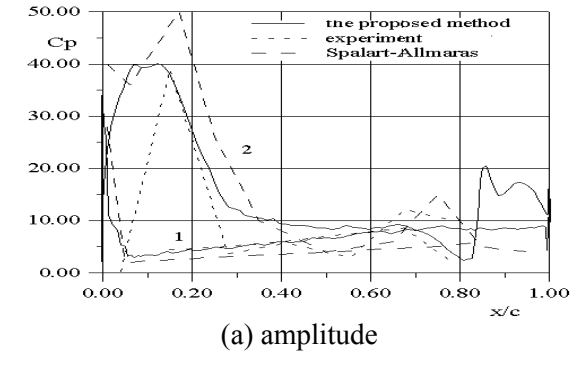

(a) amplitude

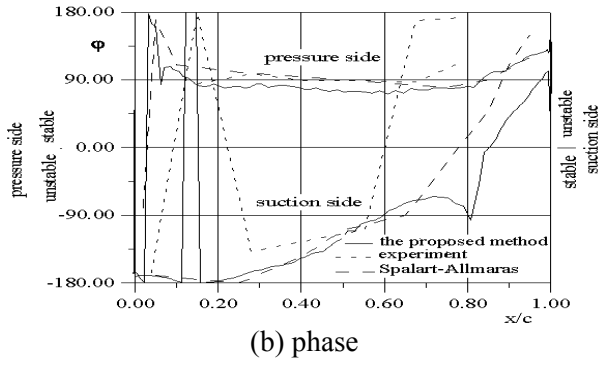

(b) phase

Figure 7: T*he phase of the 1st harmonic for unsteady pressure coefficient, IBPA=-144 deg*

We can see sufficient agreement between the method presented results, experimental data and calculated results of other authors (Cinnella et al., 2004), for the pressure distribution in the amplitude (Figures 6a, 7a) and phase (Figures 6b, 7b) for IBPA= ±144 deg. It should be noted that the results received with use of both Spalart-Allmaras and Baldwin –Lomax models compare reasonable well with experimental data except the rear part of the suction side. The discrepancies could be due to turbulence model inability to predict the position of the shock and to inaccuracy of the experimental data.

One of the basic characteristics determining the energy exchange between the gas flow and vibrating blades is the aerodamping coefficient Ξ which is equal to work coefficient of aerodynamic forces acting on the blade during a period of vibrations taken with the sign "minus". Positive values of this coefficient correspond to dissipation of vibrating blade energy in gas flow (aerodamping), negative values correspond to energy bringing to the blade (self-exciting).

For the completeness the results for the aerodamping coefficient versus IBPA are presented in Figure 8. We can observe the positive aerodamping for all values of IBPA. The graphs demonstrate a nice agreement between the method proposed and the numerical results received by FINSUP Q3D method (Fransson et al, 1999) and with use the Spalart-Allmaras turbulence model (Cinnella et al, 2004).

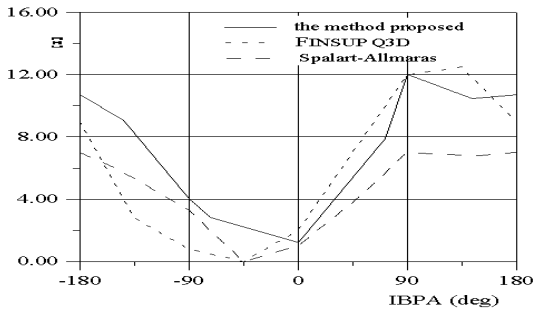

Figure 8: *The aerodamping coefficient versus IBPA*

The method proposed was used to study aeroelastic behaviour for the rotor blade row of the last stage of 200 MW steam turbine (with the length of the blade *l*=765 mm). Simulation was conducted for inviscid and viscous gas through the blades vibrating by a given harmonic law for two regimes: nominal regime with back-pressure $p_2 = 2300\,Pa$ and off-design regime with $p_2 = 9000\,Pa$. Zones of stable and unstable vibrations have been predicted.

Calculations were carried out with taking into account of the first five natural modes separately for each of the forms under different interblade phase

angles (IBPA): 0; 180; ± 90 deg. The natural modes and frequencies of the blade vibrations in vacuum were obtained with use of the finite element analysis. A more detailed description of blade geometry, natural modes of oscillations and aeroelastic behaviour with use of inviscid model was given in work (R. Rzadkowski et. al, 1999).

Figures 9,10 illustrate the dependence of the aerodamping coefficient averaged along the blade length from IBPA for each of natural modes for two regimes respectively. Squares correspond to viscous flow, rhombs correspond to inviscid gas.

All the curves are of a typical sinusoidal form. As it has seen from the graph (Figure 10) the 3rd and 4th forms may be unstable ($\Xi<0$) under the nominal regime.

Off-design regime under $p_2 = 9000\,Pa$ is characterized by considerably changed nature of aerodamping for inviscid and viscous gas. For inviscid gas all forms are damped. For viscous gas there are observed two zones of self-excitation: the 1st form under IBPA of -90 deg, and the 3rd form under IBPA of 90 deg.

The presented results show the coincidence of the calculated aerodamping coefficients in models of inviscid gas and viscous gas under the nominal regime. For a partial regime of $p_2 = 9000\,Pa$ the aerodynamic coefficients for inviscid and viscous gas are essentially different in value and under some IBPA in sign. This fact confirms that only the viscous code can predict the aeroelastic characteristics of the blade row under off-design regimes.

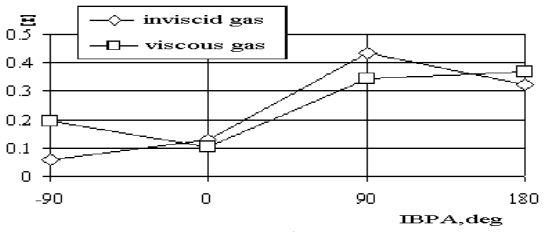

(a) 1st form, 100 Hz

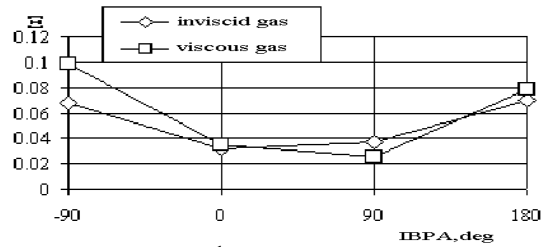

(b) 2nd form, 150 Hz

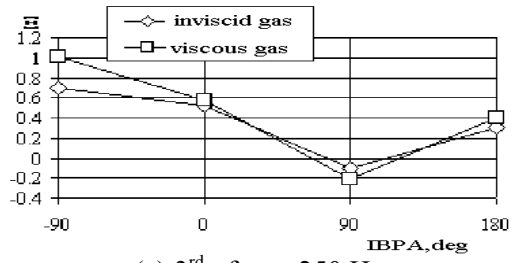

(c) 3rd form, 250 Hz

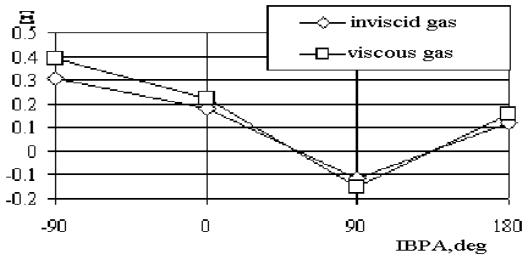

(d) 4th form, 300 Hz

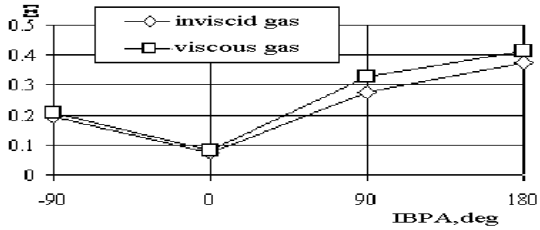

(e) 5th form, 400 Hz

Figure 9: *Dependence of aerodynamic damping from IBPA for regime p2 = 2300 Pa*

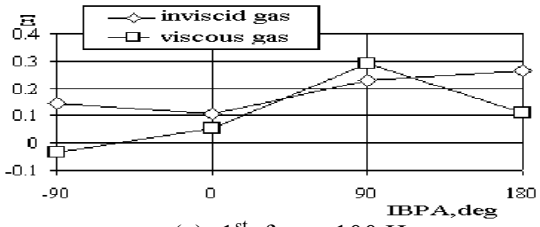

(a) 1st form, 100 Hz

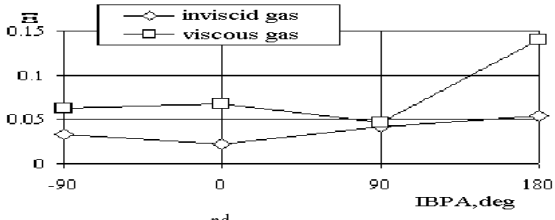

(b) 2nd form, 150 Hz

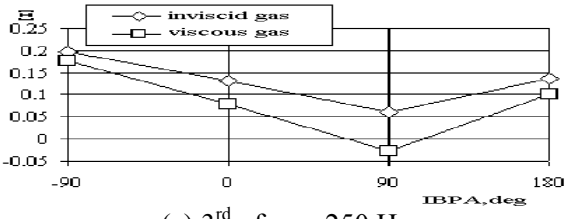

(c) 3rd form, 250 Hz

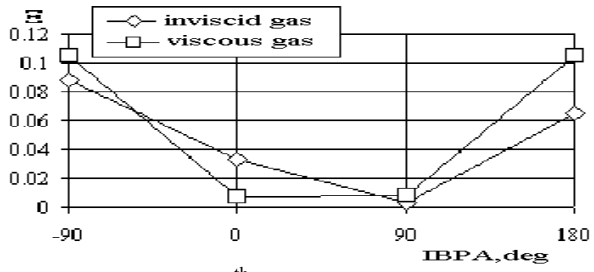

(d) 4th form, 300 Hz

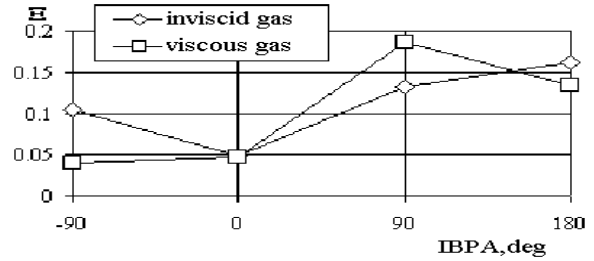

(e) 5th form, 400 Hz

Figure 10: *Dependence of aerodynamic damping from IBPA for regime p2 = 9000 Pa*

4. CONCLUSION

The numerical method to integrate the 3D Reynolds-averaged Navier-Stokes (RANS) equations with the use of a modified Baldwin and Lomax algebraic eddy viscous turbulence model applied to calculate three-dimensional unsteady viscous flow through a vibrating turbine cascade is presented.

The comparison of calculated and experimental results for the 11th Standard Configuration has shown sufficient quantitative and qualitative agreement for unsteady pressure amplitude but there are some discrepancies for the phase distribution, especially in the rear part of the suction side where a moving shock impinges on the boundary layer.

The numerical method presented here has shown some promise in being able to predict aerodamping, but the quality of the predictions has to be improved with use of more perfect turbulence models.

5. REFERENCES

Baldwin B. and Lomax L., 1978, Thin layer approximation and algebraic model for separated turbulent flow. *AIAA Paper 78-0257*.

Cebeci T. and Smith A.M.,1974, Analysis of Turbulent Boundary Layers. *N. Y., Academic Pres.*

Chassaing J.C, Gerolymos G.A., 2001, Compressor Flutter Analysis Using Time-Nonlinear and Time-Linearized 3-D Navier-Stokes Method. In *Unsteady Aerodynamics, Aeroacustics and Aeroelasticity of Turbomachines,* Proceedings of the 9th International Symposium held in Lyon, France, 4-8 September 2000, Presses Universitaires de Grenoble, 666-677.

Cinnella P. et al, 2004, A Numerical Method for Turbomachinery Aeroelasticity. *Journal of Turbomachiner,*. **126:** 310-316.

Fransson T.H. et al, 1999, Viscous and Inviscid Linear/Nonlinear Calculations Versus Quasi-Three-Dimensional Experimental Data for a New Aeroelastic Turbine Standard Configuration. *ASME Journal of Turbomachiner,* **121:** 717-725.

Gnesin V.I. et al, 2004, A numerical modelling of stator- rotor interaction in a turbine stage with oscillating blades. *Journal of Fluid and Structure,* **19:** 1141-1153.

Godunov, S. K. et al.,1976, Numerical Solution of Multidimensional Problems in Gasdynamics. *Nauka, M.*, (in Russian).

Rzadkowski R. et al, 1999, A 3D coupled fluid-structure aeroelastic analysis for turbomachinery rotor blade row. J*ournal of Mechanical Engineering,* **2:** N 3-4, 45-53.

Sayma A.I. et al, 1998, Whole -Assembly Flutter Analysis of a Low Pressure Turbine Blade. In *Unsteady Aerodynamics and Aeroelasticity of Turbomachines*, Proceedings of the 8th International Symposium held in Stockholm, Sweden, 14-18 September 1997, Kluwer Academic Publishers, 347-359.

Vasanthakumar P. et al, 2001, Three-Dimensional Viscous Computation of Blade Flutter and Forced Response Using Nonlinear Harmonic Approach. *In Unsteady Aerodynamics, Aeroacustics and Aeroelasticity of Turbomachines*, Proceedings of the 9th International Symposium held in Lyon, France, 4-8 September 2000, Presses Universitaires de Grenoble, 649-665.

Weber S. et al, 1998, Numerical Solution of the Navier Stokes Equations for Unsteady Unstalled and Stalled Flow in Turbomachniery Cascade with Oscillating Blades. In *Unsteady Aerodynamics and Aeroelasticity of Turbomachines,* Proceedings of the 8th International Symposium held in Stockholm, Sweden, 14-18 September 1997, Kluwer Academic Publishers, 478-491.